

## Dynamics of a Brownian circle swimmer

Sven van Teeffelen\* and Hartmut Löwen

Institut für Theoretische Physik II: Weiche Materie, Heinrich-Heine-Universität Düsseldorf, D-40225 Düsseldorf, Germany

(Received 13 March 2008; revised manuscript received 8 May 2008; published 15 August 2008)

Self-propelled particles move along circles rather than along a straight line when their driving force does not coincide with their propagation direction. Examples include confined bacteria and spermatozoa, catalytically driven nanorods, active, anisotropic colloidal particles and vibrated granulates. Using a non-Hamiltonian rate theory and computer simulations, we study the motion of a Brownian “circle swimmer” in a confining channel. A sliding mode close to the wall leads to a huge acceleration as compared to the bulk motion, which can further be enhanced by an optimal effective torque-to-force ratio.

DOI: 10.1103/PhysRevE.78.020101

PACS number(s): 05.40.Jc, 82.70.Dd

Active particles, which are self-propelled by their own motor, exhibit a wealth of novel and fascinating nonequilibrium effects such as giant density fluctuations [1], swarming [2], and swirling [3]. Examples are found in quite different areas of physics and include micro-organisms propelled by flagella in a fluid [4–8], man-made colloidal swimmers [9], catalytically driven nanorods or Janus particles [10,11], vibrated granulates of polar rods [3,12], and pedestrians [13]. Typically it is assumed that the swimmers move along their symmetry axis such that the force and the particle orientation are in line. This leads to a motion along a straight line just perturbed by random (e.g., Brownian) fluctuations.

Here we study the case in which the internal force propelling a colloidal particle does not coincide with the particle orientation. In the absence of Brownian fluctuations, this will lead to an overdamped motion along a closed circle, therefore we refer to this particle as a “circle swimmer.” Even a slight misalignment of the drive direction will result in circle swimming, which is thus the generic case of self-propulsion. Circle swimmers with a pronounced curved trajectory are realized in nature and can be artificially prepared: In fact, it has been shown that certain bacteria [6–8,14] and spermatozoa [4,5], when confined to two dimensions, swim in circles. Moreover, catalytically driven nanorods [10,11] and colloidal particles [9] can be prepared with a tilted motor, and a vibrated polar rod [3] on a planar substrate with an additional left-right asymmetry will move along circles. Last but not least, the trajectories of completely blinded and ear-plugged pedestrians have a significant circular form [15]. Despite their practical importance, the Brownian dynamics of a circle swimmer has not yet been addressed by theory and simulation either in the bulk or under confinement [16].

In this paper, we propose a simple model for Brownian motion of a circle swimmer in two spatial dimensions arising from the combined actions of an internal self-propelling force and a torque. We solve the Langevin equation of a two-dimensional circle swimmer analytically in the bulk providing a suitable reference model. The averaged position falls on a *spira mirabilis*, and a crossover from an oscillatory ballistic to a diffusive behavior is found in the mean-squared displacement. We then identify the modes of propagation of

a circle swimmer in confining channels with repulsive walls using computer simulations and a non-Hamiltonian rate theory. In symmetric channels, the long-time self-diffusion coefficient  $D_L$  is significantly enhanced, mediated by an efficient *sliding mode* of a tilted rod close to a wall. Furthermore,  $D_L$  is nonmonotonic in the torque. Finally, in asymmetric channels which are lacking a left-right symmetry (e.g., due to gravity [17]), the sliding mode of the circle swimmer yields a *ballistic* motion along the wall.

Neglecting hydrodynamic interactions, the overdamped motion of the Brownian circle swimmer in two dimensions (2D) is governed by the Langevin equations for the rod center-of-mass position  $\dot{\mathbf{r}} = \beta \mathbf{D} \cdot [F \hat{\mathbf{u}} - \nabla V(\mathbf{r}, \phi) + \mathbf{f}]$  and for the rod orientation  $\dot{\phi} = \beta D_r [M - \partial_\phi V(\mathbf{r}, \phi) + \tau]$ , respectively, where dots denote time derivatives and  $\beta^{-1} = k_B T$  is the thermal energy. The rod’s short time diffusion tensor  $\mathbf{D} = D_{\parallel}(\hat{\mathbf{u}} \otimes \hat{\mathbf{u}}) + D_{\perp}(\mathbf{I} - \hat{\mathbf{u}} \otimes \hat{\mathbf{u}})$  is given in terms of the short time longitudinal ( $D_{\parallel}$ ) and transverse ( $D_{\perp}$ ) translational diffusion constants, with  $\hat{\mathbf{u}} = (\cos \phi, \sin \phi)$ ,  $\mathbf{I}$  the unit tensor, and  $\otimes$  a dyadic product.  $D_r$  is the short time rotational diffusion constant.  $F \hat{\mathbf{u}}$  is a constant *effective* internal force that represents the propulsion mechanism responsible for the deterministic motion in the rod orientation, and  $M$  is a constant *effective* internal or external torque yielding the deterministic circular motion (see the sketch in Fig. 1).  $V(\mathbf{r}, \phi)$  is an external confining potential.  $\mathbf{f}$  and  $\tau$  are the zero mean Gaussian white noise random force and random torque originating from the solvent, respectively. Their variances are given by  $\overline{f_{\parallel}(t)f_{\parallel}(t')} = 2\delta(t-t')/(\beta^2 D_{\parallel})$ ,  $\overline{f_{\perp}(t)f_{\perp}(t')} = 2\delta(t-t')/(\beta^2 D_{\perp})$ , and  $\overline{\tau(t)\tau(t')} = 2\delta(t-t')/(\beta^2 D_r)$ , where  $f_{\parallel}, f_{\perp}$  are the components of  $\mathbf{f}$  parallel and perpendicular to  $\hat{\mathbf{u}}$ , respectively. The bars over the quantities denote a noise average. We remark that for an active self-propelled particle,  $F$  and  $M$  are *effective* net forces that could be determined in the bulk from the forward and angular velocities  $F = |\dot{\mathbf{r}}|/(\beta D_{\parallel})$  and  $M = |\dot{\phi}|/(\beta D_r)$ , respectively, but are not necessarily directly connected to the internal propulsion mechanism [18].

At first we consider the free circle swimmer, i.e., we set  $V(\mathbf{r}, \phi) = 0$ . In the limit of zero temperature, the rod center of mass would describe a perfect circle of radius  $R = (D_{\parallel}F)/(D_r M)$ , with the circular frequency  $\omega \equiv \beta D_r M$ . For finite temperature, all moments of  $\mathbf{r}$  and  $\phi$  can be calculated exactly. The first and second moments of  $\phi(t)$  are simply given by  $\overline{\phi} = \phi_0 + \omega t$  and  $\overline{\Delta \phi^2} = \overline{[\phi(t) - \phi_0]^2} = (\omega t)^2 + 2D_r t$ ,

\*teeffelen@thphys.uni-duesseldorf.de

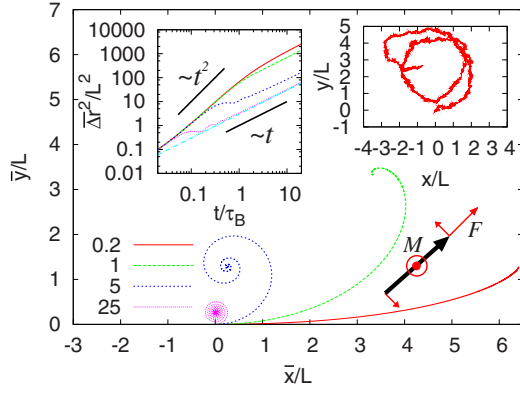


FIG. 1. (Color online) Trajectories of the mean position  $\bar{\mathbf{r}}$  of the self-propelling rod for fixed  $\beta FL=10$ ,  $\beta M=0.2, 1, 5, 25$  ( $\mathbf{r}_0=0$ ,  $\phi_0=0$ ). Left inset: the mean-square displacement  $\Delta \mathbf{r}^2$  for the same force and torques, but also for  $\beta FL=0$ ,  $\beta M=0$  (lowermost curve). Right inset: a typical trajectory of the rod for  $\beta FL=25$ ,  $\beta M=10$ , for times  $0 < t < \tau_B$ . Lower right inset: Sketch of the self-propelled circle swimmer.

where  $\phi_0 = \phi(t=0)$ , and where we let  $\phi$  run *ad infinitum*. The first two moments of  $\Delta \mathbf{r} \equiv \mathbf{r}(t) - \mathbf{r}(0)$  are given by

$$\overline{\Delta \mathbf{r}} = \lambda [D_r \hat{\mathbf{u}}_0 + \omega \hat{\mathbf{u}}_0^\perp - e^{-D_r t} (D_r \bar{\mathbf{u}} + \omega \bar{\mathbf{u}}^\perp)],$$

$$\overline{\Delta \mathbf{r}^2} = 2\lambda^2 \{ \omega^2 - D_r^2 + D_r (D_r^2 + \omega^2) t + e^{-D_r t} [(D_r^2 - \omega^2) \cos(\omega t) - 2D_r \omega \sin(\omega t)] \} + 2(D_{\parallel} + D_{\perp}) t, \quad (1)$$

with  $\lambda = \beta D_{\parallel} F / (D_r^2 + \omega^2)$ ,  $\hat{\mathbf{u}}_0 = (\cos \phi_0, \sin \phi_0)$ ,  $\hat{\mathbf{u}}_0^\perp = (-\sin \phi_0, \cos \phi_0)$ ,  $\bar{\mathbf{u}} = (\cos \bar{\phi}, \sin \bar{\phi})$ , and  $\bar{\mathbf{u}}^\perp = (-\sin \bar{\phi}, \cos \bar{\phi})$ , i.e.,  $\overline{\Delta \mathbf{r}}$  describes a *spira mirabilis*.

We consider a very thin rod of length  $L$ , where  $D_r/D_{\parallel} = 3/(2L^2)$ ,  $D_{\perp} = D_{\parallel}/2$ . We will denote all times in units of  $\tau_B = L^2/D_{\parallel}$ , lengths in units of  $L$ , and energies in units of  $\beta^{-1}$ . Different regimes are distinguished in terms of the dimensionless quantities  $D_r/\omega$  and  $\beta FL$ . The latter determines whether the rod's erratic motion is dominated by the kicks of the solvent particles or by the self-propulsion. The former is the ratio of the ballistic over the random turning rate. In Fig. 1, we show  $\overline{\Delta \mathbf{r}}$  for different internal torques  $M$  and a typical trajectory of the rod position during two complete turns. In the second inset of Fig. 1, we display  $\overline{\Delta \mathbf{r}^2}$ , which shows deterministic behavior for  $t \lesssim 1/D_r$ , while for large times the swimmer moves in a random fashion according to  $\overline{\Delta \mathbf{r}^2} \propto t$ .

Next, we introduce a confining, integrated segment-wall power-law potential in the  $x$  direction,  $V(x, \phi) = \int_0^L dl v[x'(l)] + kx$  with  $v(x') \equiv (\beta L)^{-1} \{ [L/x']^n + [L/(L_x - x')]^n \}$ , where  $L_x$  is the channel width,  $n=24$  is a large exponent, and  $x'(l)$  is the  $x$  position of the rod segment at contour length  $l$  (see the right inset of Fig. 2). In case the solvent is confined as well, hydrodynamic interactions between the particle and the wall lead in principle to an  $x$ -dependent diffusion tensor [19], which is ignored in our model. An additional gravitational force in the  $x$  direction [17] of strength  $k$  will be applied later, but we focus first on the symmetric case  $k=0$ . At zero temperature, for a not too large ratio  $M/LF$  and under appropriate initial conditions

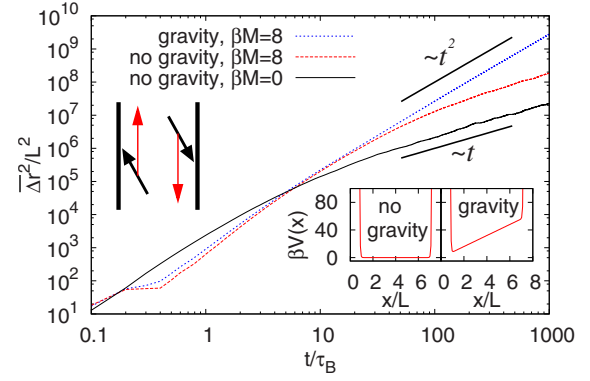


FIG. 2. (Color online) Mean-square displacement  $\overline{\Delta \mathbf{r}^2}$  in confinement ( $\beta FL=60$ ,  $L_x=8L$ ) without gravity and with zero torque (black), without gravity and with finite torque (red), and with torque and gravity (blue). The left inset displays the rod sliding along the walls. The right inset shows the confining potential without (left) and with (right) gravity.

( $\mathbf{r}_0, \phi_0$ ), the tilted swimmer performs a steady-state *sliding motion* along either of the two walls with a constant  $x$  position close to the wall and with a constant angle  $\phi$  determined by the steady-state conditions  $\dot{x}=0$  and  $\dot{\phi}=0$ , respectively. Without loss of generality, we consider the case  $M > 0$ , i.e., the rod rotates counterclockwise, such that it slides upwards along the left wall (see the sketch in Fig. 2). In the limit of hard walls ( $n \rightarrow \infty$ ), the two solutions to the set of steady-state equations can be given explicitly as  $x_{s/u} = L(1 - 1/2 \cos \phi_{s/u})$  (i.e., the front rod tip sits on the wall), and  $\cos^2 \phi_{s/u} = [1 - 2(M/LF)^2 \mp \sqrt{1 - 8(M/LF)^2}] / [2 + 2(M/LF)^2]$ ,  $\cos \phi_{s/u} < 0$ , where the minus sign corresponds to the stable ( $\phi_s$ ) and the plus sign to the unstable ( $\phi_u$ ) solution. Clearly, for  $2\sqrt{2}M/LF > 1$  there is no solution to the steady-state conditions, but the rod keeps on rotating. For large exponents  $n$ , the asymptotic steady-state velocity in the  $y$  direction is given by  $v_y \approx D_{\parallel} F \sin \phi_s / (1 + \cos^2 \phi_s)$ .

The sliding mode is also present at finite temperature. However, by thermal fluctuations the rod eventually leaves the wall and reaches the opposite wall under an appropriate angle for the respective sliding mode in the opposite  $y$  direction, which we refer to as “flipping.” Consequently, the circle swimmer moves diffusively according to  $\overline{\Delta \mathbf{r}^2} \approx 2D_L t$ , with  $D_L$  the long-time translational diffusion coefficient. This picture is clearly confirmed by Brownian dynamics computer simulations, averaged over 1000 independent simulation runs, as shown in Fig. 2.

For large  $\beta FL$ , large  $\beta M$ , and a channel width of the order of the circle radius ( $L_x \lesssim R$ ), the average time the swimmer spends in its stable mode on either of the walls is large as compared to the duration of a flip. Thus, the swimmer effectively performs a one-dimensional random walk with a typical step length  $a \approx v_y / \gamma$ , where  $\gamma$  is the flipping rate. This random walk leads to a long-time diffusion coefficient of  $D_L \approx v_y^2 / \gamma$ , which we display as a function of internal torque  $M$  for different wall-wall separations  $L_x$  in Fig. 3.

It is clearly seen from the simulations [Fig. 3(a)] that the

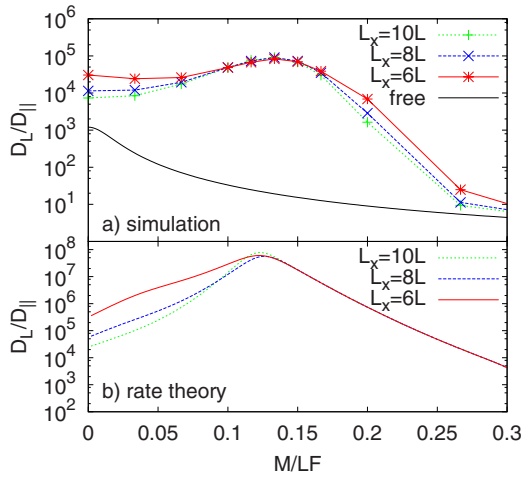


FIG. 3. (Color online) Long-time diffusion coefficient  $D_L$  as a function of the torque  $M$  for the swimmer in the bulk and in confinement for  $\beta FL=60$  and  $L_x=6, 8, 10L$ . (a) Computer simulation, (b) rate theory.

diffusion in the channel is strongly enhanced as compared to the diffusivity of the free swimmer. In particular, this strong enhancement is already observed for  $M=0$ , as the narrow walls constantly align the rod in the  $y$  direction. However, the diffusion eventually slows with increasing wall-wall separation  $L_x$ . For intermediate  $M/LF \approx 0.15$ , diffusion is enhanced even further—in the simulations [Fig. 3(a)] by an order of magnitude—displaying a much smaller dependence on  $L_x$ . This nonmonotonic behavior of  $D_L$  as a function of  $M$  is due to the stability of the sliding mode.

To understand the nontrivial interplay of  $F$ ,  $M$ , and  $L_x$  in more detail, we identified from the simulations three different paths, (a), (b), and (c), dominating the flipping rate  $\gamma$ . They all describe the transition from a stable mode at the left wall ( $\phi_s, x_s$ ) to another at the right wall ( $\phi_s + \pi, L_x - x_s$ ) due to fluctuations in the rod orientation  $\phi$ , whereas the translational motion just follows the internal force  $F$  and the confining potential  $V(\mathbf{r}, \phi)$  [20]. These three different paths are sketched in Fig. 4 and are described as follows: The rod can slip out of its stable sliding mode by fluctuating in the direction of the torque [path (a)] or by fluctuating against it [path (b)]. In path (a), detachment from the (left) wall, which amounts to overcoming a barrier in the torque/angle from  $\phi_s$  to  $\phi_u$ , most likely also leads to finding the stable mode on the other (right) wall (for  $L_x \lesssim R$ ). Path (b), however, is only successful if the rod orientation is subject to strong and fast fluctuations, which enable it to make a turn of an angle  $(-\pi + \phi_u - \phi_s)$  before reaching the other wall. This explains why for intermediate torques and small  $L_x$ , another important three-stage path (c) is dominating. This path is initiated by a small fluctuation of the orientation against the direction of the torque, from  $\phi_s$  toward  $\pi/2$  on the (left) wall. In a second stage, the swimmer approaches the other (right) wall at a small, constant turning velocity  $\dot{\phi}$ , reaching it after only a short time due to its strong internal force. By the other (right) wall it is reoriented in an upward direction before, in a third stage, turning quickly in the direction of the torque such that it reaches the original (left) wall at an angle  $\phi_u$ . The flipping

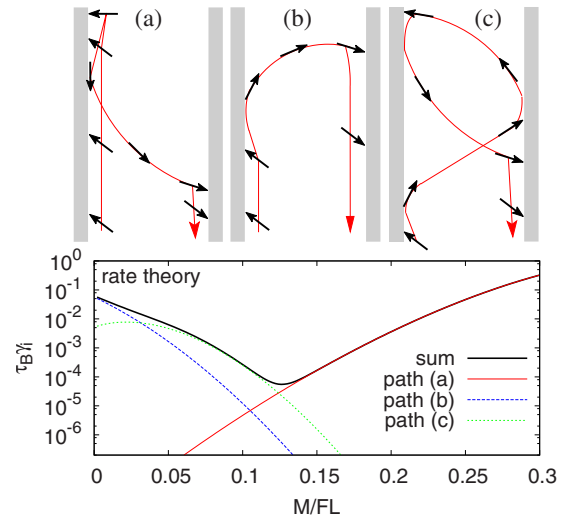


FIG. 4. (Color online) Top panel: the paths governing the flipping rate: (a) turning in the direction of the torque, (b) turning against the direction of the torque, (c) three-stage event—first, turning in the direction of the torque and then turning against it. Bottom panel: The rates of the three different paths as a function of  $M/LF$  for  $\beta FL=60$ ,  $L_x=8L$ .

rate is now given by the path integral  $\gamma \propto \int D\phi \exp(-\beta S[\mathbf{r}, \phi]/4)$ , keeping initial and final configurations of  $\phi$  and  $x$  appropriately fixed. Here, the Onsager-Machlup action is given by  $S[\mathbf{r}, \phi] = \int_0^\infty dt' |\partial_{t'} \phi(t') - M + \partial_\phi V(\mathbf{r}(t'), \phi(t'))|^2$  [21,22], with  $t' = \beta D_t t$  the normalized time. Note that our system is non-Hamiltonian due to the internal driving force and the translation-rotation coupling. Hence, the least action path cannot be found as the minimum energy path in some energy landscape, as vastly studied in the literature [23,24]. In contrast, we now construct a non-Hamiltonian rate theory by assuming that—in the limit of large forces  $\beta FL$ —the flipping rate  $\gamma$  is dominated by either of the three paths [ $i=(a), (b), (c)$ ], identified in the simulation. The respective minimum actions are given by  $S_i[\mathbf{r}_i, \phi_i]$ , with  $\phi_i(t')$  minimizing the action subject to the constraints  $[\phi_i(0) = \phi_s, x_i(0) = x_s]$  and  $[\phi_i(\infty) = \phi_s \pm \pi, x_i(\infty) = L_x - x_s]$ , where the plus sign corresponds to paths (a) and (c), and the minus sign to path (b). Paths (a) and (b) [(c)] are further constrained by the condition not to (reach) the initial wall between the initial and the final stage.

In order to calculate the associated actions for the different paths, we divide the trajectories into parts where the front rod tip sits on the original (left) wall and into parts where the rod moves at a constant turning velocity  $\dot{\phi}_i$  in between the walls. The former parts can then be expressed as the barrier heights  $4 \int \dot{\phi}_s^m d\phi |M - \partial_\phi V|$  [24], with  $\phi_m = \phi_u$  for path (a) and  $\phi_m = \pi/2$  for paths (b), (c), whereas the latter are simply given by  $|\partial_{t'} \phi_i - M|^2 t'_{\max}$ ,  $t'_{\max}$  being the normalized time it takes to swim from one wall to the other ( $t'_{\max}$  is chosen to minimize the action). The individual rates are roughly given by  $\gamma_i \approx \exp[-\beta S_i/4]/\tau_B$ , where the kinetic prefactors are crudely approximated by  $1/\tau_B$ , and plotted in Fig. 4. Summation over the individual rates yields the long-time diffusion coefficient  $D_L \approx v_y^2 \gamma^{-1}$ , with  $\gamma = \sum_i \gamma_i$  plotted as a function of  $M$  for different  $L_x$  in Fig. 3(b). The rate theory

reproduces clearly the  $L_x$  dependence and the nonmonotonicity of  $D_L$  as a function of  $M$  and attributes it to different rates of the paths (a) and (c). Moreover, the maximum in  $D_L$  is predicted to be weakly dependent on  $L_x$  in agreement with the simulations. However, the actual values of the rate theory differ from the simulation data due to the crude approximation made for the kinetic prefactors.

Finally, we study the effect of an additional gravitational field in the  $x$  direction ( $k > 0$ ), breaking the symmetry of the channel potential (see the right inset of Fig. 2). On average, the swimmer is now situated more on the left than on the right channel wall, such that the sliding mode becomes *ballistic* (see Fig. 2).

In conclusion, we have studied the dynamic behavior of a self-propelled Brownian rod performing circular motion. In the bulk, the analytical solution reveals long-time diffusive behavior. In channel confinement, an efficient stable sliding mode was identified that strongly enhances the long-time diffusion along the channel as obtained by computer simulation and a non-Hamiltonian rate theory. If the channel is asymmetric, the sliding mode leads to ballistic long-time motion.

The sliding motion of circle swimmers can be verified in experiments with different setups: First, catalytically driven nanorods [10,11] and self-propelled magnetic colloidal rods confined to a microchannel [17] will exhibit sliding [25].

Second, confined bacteria [6–8] and spermatozoa [4,5] move in two dimensions along circles. In fact, the typical radius of the observed circular motion is in the range of 10–1000  $\mu\text{m}$  for spermatozoa [4,5] and of the order of 50  $\mu\text{m}$  for *Escherichia coli* bacteria [8]. Therefore, the radii are typically larger but comparable with the particle sizes. When these particles are exposed to microchannels of similar widths as the observed radii, as realized for the bacteria [6], the predicted huge acceleration behavior should be observed, as has already been seen in 3D [8]. Third, vibrated polar granular rods [3] with an additional left-right asymmetry perform circle motions. When placed into a slit geometry, a sliding effect may be observed here as well.

Accelerating the dynamics in the channel by tuning the torque may be exploited as a mechanism to separate a certain species out of a crowded solution of different active particles. If a microfluidic channel is connected to a bulk mixture, the species moving quickest along the channel will arrive first at the channel end and can efficiently be removed. This might be more efficient than traditional separation techniques such as capillary electrophoresis [26].

We thank U. Zimmermann, H. H. Wensink, A. Wynveen, and W. C. K. Poon for helpful discussions. This work has been supported by the DFG through the SFB TR6 (project C3).

- 
- [1] R. A. Simha and S. Ramaswamy, *Phys. Rev. Lett.* **89**, 058101 (2002).
- [2] T. Vicsek, A. Czirok, E. Ben-Jacob, I. Cohen, and O. Shochet, *Phys. Rev. Lett.* **75**, 1226 (1995).
- [3] A. Kudrolli, G. Lumay, D. Volfson, and L. S. Tsimring, *Phys. Rev. Lett.* **100**, 058001 (2008).
- [4] I. H. Riedel, K. Kruse, and J. Howard, *Science* **309**, 300 (2005).
- [5] D. M. Woolley, *Reproduction (Bristol, U.K.)* **126**, 259 (2003).
- [6] W. R. DiLuzio *et al.*, *Nature* **435**, 1271 (2005).
- [7] J. Hill, O. Kalkanci, J. L. McMurry, and H. Koser, *Phys. Rev. Lett.* **98**, 068101 (2007).
- [8] H. C. Berg and L. Turner, *Biophys. J.* **58**, 919 (1990).
- [9] R. Dreyfus *et al.*, *Nature* **437**, 862 (2005).
- [10] P. Dhar *et al.*, *Nano Lett.* **6**, 66 (2006).
- [11] A. Walther and A. H. E. Müller, *Soft Matter* **4**, 663 (2008).
- [12] V. Narayan, S. Ramaswamy, and N. Menon, *Science* **317**, 105 (2007).
- [13] D. Helbing, *Rev. Mod. Phys.* **73**, 1067 (2001).
- [14] E. Lauga *et al.*, *Biophys. J.* **90**, 400 (2006).
- [15] T. Obata *et al.*, *J. Korean Phys. Soc.* **46**, 713 (2005).
- [16] We note that in three spatial dimensions, misalignment of internal direction and force leads to motion along spirals, which has been observed for bacteria; see V. B. Shenoy *et al.*, *Proc. Natl. Acad. Sci. U.S.A.* **104**, 8229 (2007).
- [17] M. Köppl, P. Henseler, A. Erbe, P. Nielaba, and P. Leiderer, *Phys. Rev. Lett.* **97**, 208302 (2006).
- [18] O. Raz and J. E. Avron, *New J. Phys.* **9**, 437 (2007).
- [19] E. R. Dufresne, T. M. Squires, M. P. Brenner, and D. G. Grier, *Phys. Rev. Lett.* **85**, 3317 (2000).
- [20] This assumption is clearly justified for large ratios  $D_r/D_{\parallel}$ ,  $D_r/D_{\perp} \gg 1/L^2$ , and  $FL/M \gg 1$ .
- [21] L. Onsager and S. Machlup, *Phys. Rev.* **91**, 1505 (1953).
- [22] For a recent generalization of the Onsager-Machlup theory to nonequilibrium steady states, see T. Taniguchi and E. G. D. Cohen, *J. Stat. Phys.* **126**, 1 (2007).
- [23] E. Vanden-Eijnden and M. Heymann, *J. Chem. Phys.* **128**, 061103 (2008).
- [24] R. Olender and R. Elber, *J. Mol. Struct.: THEOCHEM* **63**, 398 (1997).
- [25] F. S. Merkt *et al.*, *New J. Phys.* **8**, 216 (2006).
- [26] M. A. Rodriguez and D. W. Armstrong, *J. Chromatogr., B: Biomed. Appl.* **800**, 7 (2004).